Wave-equation Hessian by phase encoding

Yaxun Tang, Stanford University*

SUMMARY

I demonstrate a method for computing wave-equation Hessian operators, also known as resolution functions or point-spread functions, under the Born approximation. The proposed method modifies the original explicit Hessian formula, enabling efficient computation of the operator. A particular advantage of this method is that it reduces or eliminates storage of Green's functions on the hard disk. The modifications, however, also introduce undesired cross-talk artifacts. I introduce two different phase-encoding schemes, namely, plane-wave phase encoding and random phase encoding, to suppress the cross-talk. I applied the Hessian operator obtained by using random phase encoding to the Sigsbee2A synthetic data set, where a better subsalt image with higher resolution is obtained.

INTRODUCTION

Migration is an important tool for imaging subsurface structures using reflection seismic data. The classic imaging principle (Claerbout, 1971) for shot-based migration states that reflectors are located where the forward-propagated source wavefield correlates with the backward-propagated receiver wavefield. However, it has been found that such an imaging principle is only the adjoint of the forward Born modeling operator (Lailly, 1983), which provides reliable structural information of the subsurface but distorts the amplitude of the reflectors because of the non-unitary nature of the Born modeling operator. To improve relative amplitude behavior, the imaging problem can be formulated as an inverse problem based on the minimization of a least-squares functional. The inverse problem can be formulated either in the data space (Lailly, 1983; Tarantola, 1984) or in the model space (Beylkin, 1985; Chavent and Plessix, 1999; Plessix and Mulder, 2004; Valenciano et al., 2006; Yu et al., 2006). The data-space approach can be solved iteratively using the gradient-based method (Nemeth et al., 1999; Clapp, 2005) without explicit construction of the Hessian, the matrix of the second derivatives of the error functional with respect to the model parameters. The iterative solving, however, is relatively costly and converges very slowly.

On the other hand, the model-space approach requires the explicit construction of the Hessian, and its pseudo-inverse is applied to the migrated image. The full Hessian is too big and expensive to be computed in practice; hence Chavent and Plessix (1999); Plessix and Mulder (2004) approximate it by a diagonal matrix. In the case of high-frequency asymptotics, and with an infinite aperture, the Hessian is diagonal in most cases (Beylkin, 1985). For a finite range of frequencies and limited acquisition geometry, however, the Hessian is no longer diagonal and not even diagonally dominated (Plessix and Mulder, 2004; Valenciano et al., 2006). It has been shown by Valenciano et al. (2006) that, in areas of poor illumination, e.g., subsalt regions, the Hessian's main diagonal energy is smeared along its off-diagonals. Therefore, the migrated image pre-multiplied by a diagonal matrix cannot perfectly recover the amplitude information, especially in poorly illuminated areas. That's why Valenciano et al. (2006) suggest computing a limited number of the Hessian off-diagonals to compensate for poor illumination and improve the inversion result. However, computing the Hessian off-diagonals, even for a limited number, is very expensive by directly implementing the explicit Hessian formula. A huge number of Green's functions (which can easily be several hundred terabytes for a typical 3-D survey) must be precomputed and stored, and then retrieved from the disk to generate the Hessian. Such operations not only require high-volume storage, but also high-speed I/O and network. Though computer speed continues to improve rapidly, it is still a challenge to compute such a huge matrix.

To make the Hessian computation more affordable, I describe a method based on the phase-encoding technique. In this method, the original explicit Hessian formula is slightly modified to enable efficient computation of the Hessian operator. The proposed method makes the Hessian computation similar to the shot-profile migration but with slightly modified imaging conditions. The new method eliminates the need to precompute and store Green's functions, but it also introduces cross-talk artifacts. I introduce two phase-encoding schemes, plane-wave phase encoding and random phase encoding to attenuate the cross-talk. I also apply the phase-encoded Hessian to the Sigsbee2A model, where a better subsalt image with higher resolution is obtained.

LEAST-SQUARES HESSIAN

Primaries can be generated using the Born forward modeling equation:

$$d(\mathbf{r}_k,\mathbf{s}_i,\omega)=\omega^2\sum_{l=1}^{L} f_s(\omega)G_i(\mathbf{s}_i,\mathbf{x}_l,\omega)G_i(\mathbf{x}_l,\mathbf{r}_k,\omega)m(\mathbf{x}_l), \quad (1)$$

where $d(\mathbf{r}_k,\mathbf{s}_i,\omega)$ is the modeled seismic data for receiver location $\mathbf{r}_k$ $(k=1,\cdots,M)$ and shot location $\mathbf{s}_i$ $(i=1,\cdots,N)$ for a single frequency ω, $f_s(\omega)$ is the source signature. $m(\mathbf{x}_l)$ $(l=1,\cdots,L)$ is the reflectivity at $\mathbf{x}_l$ in the subsurface, $G_i(\mathbf{s}_i,\mathbf{x}_l,\omega)$ is the monochromatic Green's function from the source $\mathbf{s}_i$ to the image point $\mathbf{x}_l$ for the ith shot, and $G_i(\mathbf{x}_l,\mathbf{r}_k,\omega)$ is the monochromatic Green's function from the image point $\mathbf{x}_l$ to the receiver $\mathbf{r}_k$ for the ith shot. To invert for the reflectivity, we formulate an objective function in the least-square sense as follows:

$$F(\mathbf{m})=||\mathbf{L}\mathbf{m}-\mathbf{d}_{obs}||_2, \quad (2)$$

where $\mathbf{L}$ is the forward modeling operator defined in equation 1, $\mathbf{d}_{obs}$ is the observed data vector, and $||\cdot||_2$ stands for the L_2 norm. Instead of minimizing objective function F using the gradient-based method directly in the data space (Nemeth et al., 1999; Clapp, 2005), we reformulate it and solve it in the model space. $\mathbf{L}$ is a linear operator, so F is a quadratic function. Its minimum can be obtained when $\mathbf{m}$ satisfies:

$$\mathbf{m}=\mathbf{H}^{-1}\mathbf{L}'\mathbf{d}_{obs}, \quad (3)$$

where $'$ stands for the complex conjugate and $\mathbf{H}=\mathbf{L}'\mathbf{L}$ is the Hessian operator. Equation 3 can be rewritten as follows by recognizing that $\mathbf{L}'\mathbf{d}_{obs}$ is the migrated image $\mathbf{m}_{mig}$:

$$\mathbf{H}\mathbf{m}=\mathbf{m}_{mig}. \quad (4)$$

Now we can formulate our new objective function

$$J(\mathbf{m})=||\mathbf{H}\mathbf{m}-\mathbf{m}_{mig}||_2. \quad (5)$$

Equation 5 says that once we explicitly compute the Hessian operator $\mathbf{H}$ (which I will discuss efficient methods in later sections), we can use the linear conjugate gradient or any other method to minimize the new objective function J defined in equation 5.

The Hessian can be explicit computed with the following formula (Plessix and Mulder, 2004; Valenciano et al., 2006):

$$H(\mathbf{x}_p,\mathbf{x}_q) = \sum_{\omega}\omega^4\sum_{i=1}^{N}|f_s(\omega)|^2 G_i(\mathbf{s}_i,\mathbf{x}_p,\omega)G_i'(\mathbf{s}_i,\mathbf{x}_q,\omega) \sum_{k=1}^{M} G_i(\mathbf{r}_k,\mathbf{x}_p,\omega)G_i'(\mathbf{r}_k,\mathbf{x}_q,\omega) \quad (6)$$

Hereafter, I will call $H(\mathbf{x}_p,\mathbf{x}_q)$ in equation 6 the exact Hessian, since it is derived strictly from the least-squares functional F. It is cumbersome and very expensive to compute the exact Hessian by directly implementing the above equation, because large storage of Green's function is needed, which can require several hundred terabytes of storage space for a typical 3-D seismic survey. In the subsequent sections, I introduce an alternative method based on phase encoding for computing the Hessian operator, which reduces the computational requirement. As I will demonstrate, by using this approach, we do not need to save any Green's functions, and the cost for computing the Hessian is also significantly reduced.

PHASE-ENCODED HESSIAN

Encode the receiver-side Green's functions

Suppose we have the following function:

$$H'(\mathbf{x}_p,\mathbf{x}_q) = \sum_{\omega}\omega^4\sum_{i=1}^{N}|f_s(\omega)|^2 G_i(\mathbf{s}_i,\mathbf{x}_p,\omega)G_i'(\mathbf{s}_i,\mathbf{x}_q,\omega) \sum_{u=1}^{M} G_i(\mathbf{r}_u,\mathbf{x}_p,\omega)\alpha_u(\omega)\sum_{v=1}^{M} G_i'(\mathbf{r}_v,\mathbf{x}_q,\omega)\alpha_v'(\omega), \quad (7)$$

where an extra summation $\sum_{v=1}^{M}$ for the receiver-side Green's functions has been introduced; $\alpha_u(\omega)$ and $\alpha_v(\omega)$ are some weighting functions, which will be specified later. Equation 7 can be directly implemented by storing the Green's functions, just as with the implementation of equation 6. However, equation 7 offers more flexibility and can be very efficiently implemented without explicitly saving the Green's functions.

With the extra summation, the term $\sum_{u=1}^{M} G_i(\mathbf{r}_u,\mathbf{x}_p,\omega)\alpha_u(\omega)$ can now be seen as the extrapolated wavefield at image point $\mathbf{x}_p$, with the composite source as the source function ($f_c(\mathbf{r}_u,\omega)=\alpha_u(\omega)$, $u=1,\cdots,M$). The same thing holds for the other summation term $\sum_{v=1}^{M} G_i'(\mathbf{r}_v,\mathbf{x}_q,\omega)\alpha_v'(\omega)$, except that it is the complex conjugate of the extrapolated wavefield at image point $\mathbf{x}_q$. To make it clearer, we define the receiver wavefield $R_i(\mathbf{x},\omega)=\sum_{u=1}^{M} G_i(\mathbf{r}_u,\mathbf{x},\omega)\alpha_u(\omega)$, and the source wavefield $S_i(\mathbf{x},\omega)=f_s(\omega)G_i(\mathbf{s}_i,\mathbf{x},\omega)$. Then equation 7 becomes

$$H'(\mathbf{x}_p,\mathbf{x}_q)=\sum_{\omega}\omega^4\sum_{i=1}^{N} S_i(\mathbf{x}_p,\omega)S_i'(\mathbf{x}_q,\omega)R_i(\mathbf{x}_p,\omega)R_i'(\mathbf{x}_q,\omega), \quad (8)$$

which means $H'(\mathbf{x}_p,\mathbf{x}_q)$ can be computed by cross-correlating the source and receiver wavefields with their shifted complex conjugates ($\mathbf{x}_q$ is the neighbourhood point around $\mathbf{x}_p$). It is similar to the wave-equation shot-profile migration, except the imaging condition is slightly modified. In other words, we do not have to save the Green's functions. Instead, we can replace each shot gather with composite sources, then extrapolate it into the subsurface and use the imaging condition defined in equation 8 to generate $H'(\mathbf{x}_p,\mathbf{x}_q)$. This process is efficient because multiple Green's functions are computed at the same time during the wavefield extrapolation. It can be shown that if we let the weighting function $\alpha_k(\omega)$ satisfy $|\alpha_k(\omega)|=1$, equation 7 can be simplified as follows:

$$H'(\mathbf{x}_p,\mathbf{x}_q)=H(\mathbf{x}_p,\mathbf{x}_q)+C'(\mathbf{x}_p,\mathbf{x}_q) \quad (9)$$

where the first term is the exact Hessian, while the second term $C'(\mathbf{x}_p,\mathbf{x}_q)$ is the undesired cross-talk from the cross-correlations among different receiver-side Green's functions.

Encode the source-side and receiver-side Green's functions simultaneously

We can further encode the source-side Green's functions by synthesizing composite sources from the source locations. For simplicity, we assume Ocean Bottom Cable (OBC) or land acquisition geometry, where all the shots share the same receiver array. Therefore: $G_i(\mathbf{s}_i,\mathbf{x},\omega)=G(\mathbf{s}_i,\mathbf{x},\omega)$ and $G_i(\mathbf{r}_k,\mathbf{x},\omega)=G(\mathbf{r}_k,\mathbf{x},\omega)$. Then the following function can be constructed:

$$H''(\mathbf{x}_p,\mathbf{x}_q) = \sum_{\omega}\omega^4|f_s(\omega)|^2 \sum_{i=1}^{N} G(\mathbf{s}_i,\mathbf{x}_p,\omega)\beta_i(\omega)\sum_{j=1}^{N} G'(\mathbf{s}_j,\mathbf{x}_q,\omega)\beta_j'(\omega) \sum_{u=1}^{M} G(\mathbf{r}_u,\mathbf{x}_p,\omega)\alpha_u(\omega)\sum_{v=1}^{M} G'(\mathbf{r}_v,\mathbf{x}_q,\omega)\alpha_v'(\omega), \quad (10)$$

where two extra summations have been introduced: $\sum_{j=1}^{N}$ for the source-side Green's functions and $\sum_{v=1}^{M}$ for the receiver-side Green's functions. Let us once again define the composite source wavefield $S(\mathbf{x},\omega)=f_s(\omega)\sum_{i=1}^{N} G(\mathbf{s}_i,\mathbf{x},\omega)\beta_i(\omega)$ and composite receiver wavefield $R(\mathbf{x},\omega)=\sum_{u=1}^{M} G(\mathbf{r}_u,\mathbf{x},\omega)\alpha_u(\omega)$. Then equation 10 can be rewritten as follows:

$$H''(\mathbf{x}_p,\mathbf{x}_q)=\sum_{\omega}\omega^4 S(\mathbf{x}_p,\omega)S'(\mathbf{x}_q,\omega)R(\mathbf{x}_p,\omega)R'(\mathbf{x}_q,\omega) \quad (11)$$

Equation 11 tells us that to compute the simultaneously encoded Hessian $H''(\mathbf{x}_p,\mathbf{x}_q)$, only two wavefield propagations are required. It can also be proved that if we can choose proper weighting functions $\alpha_k(\omega)$ and $\beta_i(\omega)$ such that $|\alpha_k(\omega)|=1$ and $|\beta_i(\omega)|=1$, equation 10 becomes the summation of the exact Hessian $H(\mathbf{x}_p,\mathbf{x}_q)$ and the cross-talk $C''(\mathbf{x}_p,\mathbf{x}_q)$

$$H''(\mathbf{x}_p,\mathbf{x}_q)=H(\mathbf{x}_p,\mathbf{x}_q)+C''(\mathbf{x}_p,\mathbf{x}_q) \quad (12)$$

From equations 9 and 12, we find that we face a similar situation encountered in phase-encoding migration (Romero et al., 2000); i.e., our exact Hessian is contaminated by cross-talk artifacts, so we seek to define weighting functions $\alpha_k(\omega)$ and $\beta_i(\omega)$ that attenuate the cross-talk as much as possible. In the next two sections, I introduce two different phase-encoding schemes to attenuate the cross-talk, namely, plane-wave phase encoding and random phase encoding.

PLANE-WAVE PHASE ENCODING

Suppose we choose the weighting functions to be

$$\alpha_k(\omega)=A_r(\omega)e^{\iota\omega p_r(\mathbf{r}_k-\mathbf{r}_0)}, \beta_i(\omega)=A_s(\omega)e^{\iota\omega p_s(\mathbf{s}_i-\mathbf{s}_0)}, \quad (13)$$

which are the known plane-wave phase-encoding functions (Whitmore, 1995; Liu et al., 2006), where $A_r(\omega)$ and $A_s(\omega)$ are real functions, $\iota=\sqrt{-1}$; p_r and p_s are the ray parameters for the receiver

and source plane waves; $\mathbf{r}_0$ and $\mathbf{s}_0$ are reference locations. Here I limit my discussion to 2-D, so p_r and p_s are scalars, but it should be very straightforward to extend the analysis to 3-D. As prove by Liu et al. (2006), by summing an infinite number of plane waves ranging from $-\infty$ to $+\infty$, the cross-talk in the plane-wave migration can be completely attenuated. The same property holds here in the scenario of Hessian computation. It can be proved that by stacking over p_r and p_s, and choosing $A_r(\omega)$ and $A_s(\omega)$ to satisfy $|\omega|^{-1}A_r^2(\omega)=1$ and $|\omega|^{-1}A_s^2(\omega)=1$ respectively, the approximate Hessians $H'(\mathbf{x}_p,\mathbf{x}_q)$ and $H''(\mathbf{x}_p,\mathbf{x}_q)$ converge to the exact Hessian $H(\mathbf{x}_p,\mathbf{x}_q)$.

RANDOM PHASE ENCODING

Instead of using the plane-wave phase-encoding functions, we can use random phases to disperse these unwanted crossterms. By doing so, we don't need to stack over many p_rs or p_ss to attenuate the cross-talk, so the cost is significantly reduced. The weighting functions can be choosen as follows:

$$\alpha_u(\omega)=e^{\iota\gamma_u(\omega)},\beta_i(\omega)=e^{\iota\gamma_i(\omega)}. \tag{14}$$

where the phase functions $\gamma_u(\omega)$ and $\gamma_i(\omega)$ are sequences of random numbers between 0 and 2π. When we sum over ω to generate the final result, the phases of the cross-talk will not agree, and consequently, the cross-talk will be attenuated. To maximize the phase differences from each frequency, a uniformly distributed random sequence could be used.

NUMERICAL EXAMPLES

Verification of the algorithm: A constant velocity model

I verified the proposed phase-encoding algorithms on a constant velocity model ($v=2000$ m/s). The acquisition geometry contains only one shot at -600 meters and two receivers at 600 meters and 1200 meters on the surface. The frequency band of the seismic experiment is $5-35$ Hz, and all the frequencies are used to generate the following results. Figure 1 shows the diagonal of the Hessian (when $\mathbf{x}_p=\mathbf{x}_q$), and Figure 2 shows the Hessian with its off-diagonals (with size 21×21) at the image point $x=680$ meters, $z=800$ meters. The horizontal and vertical axes in Figure 2 are the horizontal and vertical offsets away from that image point. In both figures, panel (a)s are the exact Hessian, uncontaminated by any cross-talk. Panel (b)s are obtained by directly implementing equation 7. No weighting functions are applied ($\alpha_k(\omega)=1$), so the results are contaminated by strong cross-talk. Panel (c)s are obtained by using the plane-wave phase encoding after stacking 61 receiver-side-encoded plane waves. Panel (d)s show the results of the random phase encoding. Both phase-encoding schemes successfully remove the cross-talk shown in panel (b)s.

Inversion with the phase-encoded Hessian: The Sigsbee2A velocity model

To demonstrate the power of inversion, I applied the model-space inversion approach to the Sigsbee2A model. The explicit Hessian operator is computed by using the random phase-encoding method with the frequency band from 5 Hz to 35 Hz, which is equivalent to the frequency band of the migrated image $\mathbf{m}_{mig}$. Two different strategies have been applied: the first is to compute only the diagonal of the Hessian operator and use it to normalize the migrated image; the other is to compute the Hessian operator, including a limited number of its off-diagonals, and then use the linear conjugate gradient method to invert for the reflectivity $\mathbf{m}$.

Figure 3(a) shows the diagonal of the Hessian using random phase encoding. Note the uneven illumination caused by the complex salt body and limited acquisition geometry. For comparison, Figure

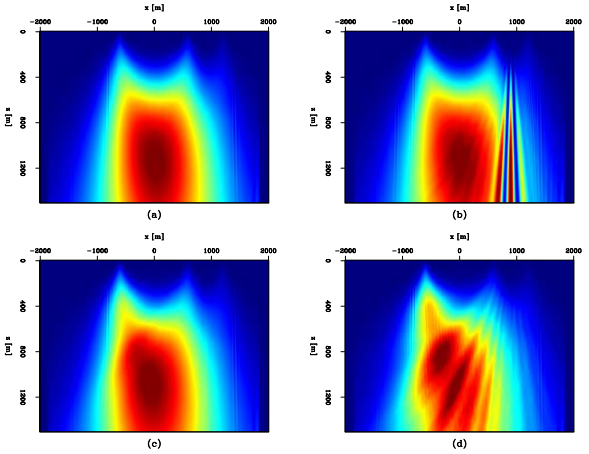

Figure 1: The diagonal of the Hessian. Panel (a) shows the exact diagonal of the Hessian; (b) shows the diagonal of the Hessian with cross-talk; (c) is obtained by using plane-wave phase encoding; (d) is obtained by using random phase encoding.

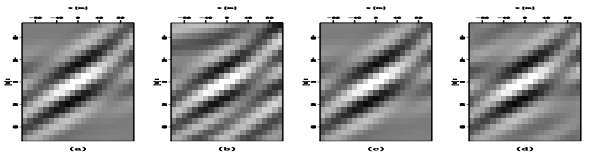

Figure 2: The Hessian operator with its off-diagonals for a particular image point. Panel (a) shows the exact Hessian operator; (b) shows the diagonal of the Hessian with cross-talk; (c) is obtained by using plane-wave phase encoding; (d) is obtained by using random phase encoding.

3(b) shows the source intensity, which is a crude approximation to the exact diagonal of Hessian. It assumes the receiver-side Green's functions to be constant, so it ignores the effects of the limited receiver arrays. It over-estimates the total energy that enters the earth and returns to be recorded by the receivers. That is why Figure 3(b) shows a better, but inaccurate, illumination coverage below the salt.

Figure 4(a) shows the conventional shot-profile migrated image, where the shadow zones below the salt can be easily identified; Figure 4(b) shows the result of normalizing the migrated image with the diagonal of the Hessian shown in Figure 3(a). For comparison, Figure 4(c) shows the result of normalizing the migrated image with the source intensity shown in Figure 3(b). Figure 4(b) shows slightly more balanced amplitude across the section than Figure

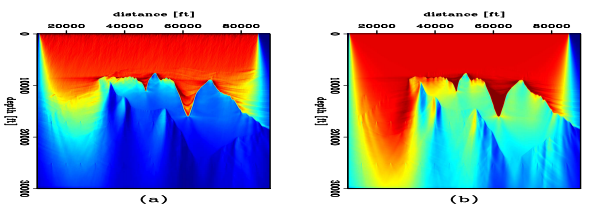

Figure 3: Panel (a) is the diagonal of the Hessian obtained by random phase encoding; (b) is the source intensity.

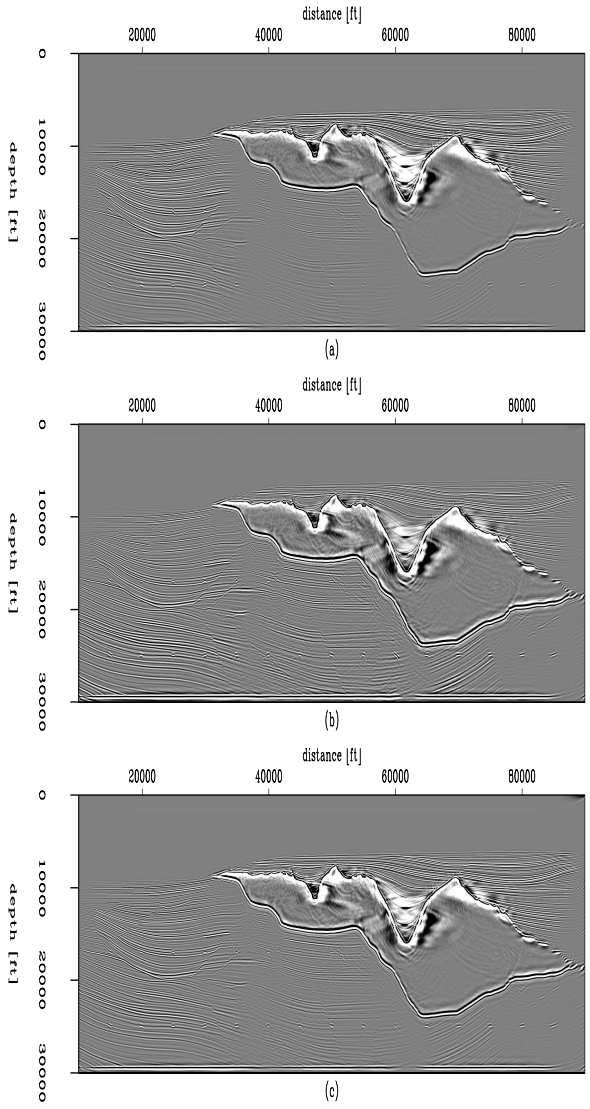

Figure 4: Panel (a) is the migration $\mathbf{m}_{mig}$; (b) is $\mathbf{m}_{mig}$ normalized with the Hessian diagonal, while (c) with the source intensity.

4(c), especially in areas below the salt. This is because Figure 3(a) takes the limited receiver arrays into consideration, and hence better predicts the illumination pattern in the subsurface.

Figure 5 is obtained by convolving the Hessian operator (with a size 21×21) with a collection of point scatters in the model space. It demonstrates the varying shapes and non-stationarity of the Hessian operator across the model space. Note that in well-illuminated areas, the Hessian operator is well focused, while in poorly illuminated areas, the Hessian operator has a preferred dipping orientation, which means these image points are illuminated by only a few dip angles. Figure 6(b) shows the inverted image obtained by using the randomly phase-encoded Hessian operator. The result is obtained after 20 iterations of the linear conjugate-gradient method. For comparison, Figure 6(a) shows the migrated image. In the inversion result, the vertical resolution is greatly enhanced; the shadow zones that in the migrated image are now filled in with structures; the sediments and the large dipping fault extend closer to the salt body. However, the inversion result also shows increased

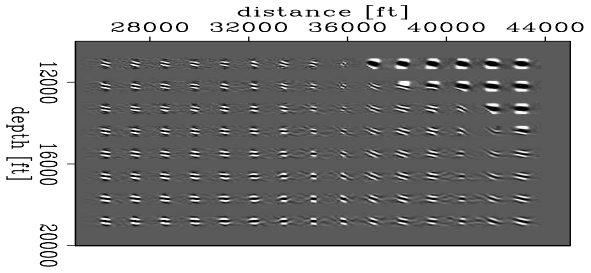

Figure 5: Convolution result of the Hessian with a collection of point scatters, it demonstrates the varying shapes of the Hessian.

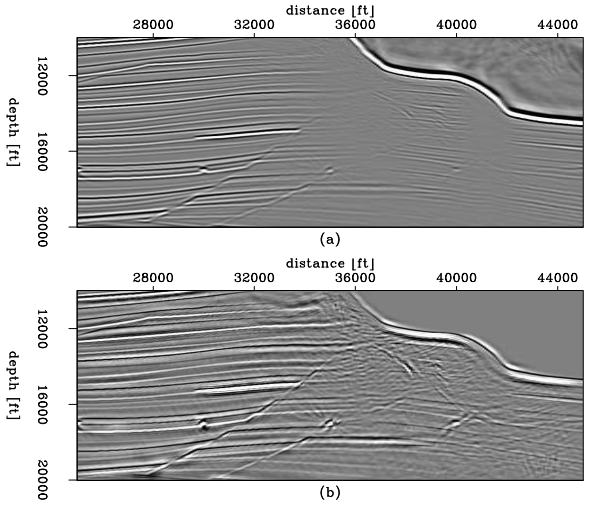

Figure 6: Panel (a) shows the shot-profile migration result, and (b) shows the inversion result with the Hessian obtained by using random phase encoding.

noise, which might be caused by the null space or the random noise introduced in the randomly phase-encoded Hessian, or both. To suppress the noise, a proper regularization term can be introduced in the inversion process.

CONCLUSION

I have introduced a method based on phase encoding that allows efficient computation of the explicit Hessian operator. The proposed algorithm closely resembles shot-profile migration, except that a slightly different imaging condition has been used, so that no Green's functions need to be pre-computed and saved on the hard disk; hence, Hessians with larger model spaces and more frequencies can be obtained. However, this method also generates undesired cross-talk. Plane-wave phase encoding and random phase encoding have been introduced to attenuate the cross-talk. Numerical examples demonstrate that these two phase-encoding schemes work well in suppressing the cross-talk. The inversion examples of using the randomly phase-encoded Hessian on the Sigsbee2A model also show promising results.

ACKNOWLEDGEMENT

The author would like to thank the sponsors of the Stanford Exploration Project for their financial support.

EDITED REFERENCES

Note: This reference list is a copy-edited version of the reference list submitted by the author. Reference lists for the 2008 SEG Technical Program Expanded Abstracts have been copy edited so that references provided with the online metadata for each paper will achieve a high degree of linking to cited sources that appear on the Web.

REFERENCES

Beylkin, G., 1985, Imaging of discontinuities in the inverse scattering problem by inversion of a causal generalized radon transform: Journal of Mathematical Physics, **26**, 99–108.

Chavent, G., and R.-E. Plessix, 1999, An optimal true-amplitude least-squares prestack depth-migration operator: Geophysics, **64**, 508–515.

Claerbout, J. F., 1971, Toward a unified theory of reflector mapping: Geophysics, **36**, 467–481.

Clapp, M. L., 2005, Imaging under salt: Illumination compensation by regularized inversion: Ph.D. thesis, Stanford University.

Lailly, P., 1983, The seismic inverse problem as a sequence of before stack migration: Proceedings of the Conference on Inverse Scattering, Theory and Applications, SIAM.

Liu, F., D. W. Hanson, et al., 2006, Toward a unified analysis for source plane-wave migration: Geophysics, **71**, S129–S139.

Nemeth, T., C. Wu, and G. Schuster, 1999, Least-squares migration of incomplete reflection data: Geophysics, **64**, 208–221.

Plessix, R.-E., and W. A. Mulder, 2004, Frequency-domain finite-difference amplitude-preserving migration: Geophysics Journal International, **157**, 975–987.

Romero, L. A., D. C. Ghiglia, C. C. Ober, and S. A. Morton, 2000, Phase encoding of shot records in prestack migration: Geophysics, **65**, 426–436.

Tarantola, A., 1984, Inversion of seismic reflection data in the acoustic approximation: Geophysics, **49**, 1259–1266.

Valenciano, A. A., B. Biondi, and A. Guitton, 2006, Target-oriented wave-equation inversion: Geophysics, **71**, A35–A38.

Whitmore, N. D., 1995, An imaging hierarchy for common-angle plane-wave seismogram: Ph.D. thesis.

Yu, J., J. Hu, G. T. Schuster, and R. Estill, 2006, Prestack migration deconvolution: Geophysics, **71**, S53–S62.